Real-Time Finite-Element Simulation of Electromagnetic Transients of Transformer on FPGA

Peng Liu, *Student Member, IEEE* and Venkata Dinavahi, *Senior Member, IEEE*

***Abstract*—The computation of the electromagnetic transients in a power transformer with nonlinear material using the finite element method (FEM) is so dense that the traditional nonlinear solver employing the Newton–Raphson method can hardly execute in real time. In this paper, we emulate the finite-element computation of electromagnetic transients of a transformer in real time for the first time. The transmission line modeling (TLM) method employed in the FEM successfully decoupled the nonlinear elements from the linear network so the nonlinearities could be solved individually, which is perfect for parallel processing. The parallelism of the TLM-FE solution is sufficiently explored and realized on a field-programmable gate array with deep data pipelining, and the implementation can execute in real time and provide detailed field information of the transformer during the transients. The proposed noniterative field–circuit coupling enabled the transformer to interface with an external network and the comparison with commercial FEM software proved the accuracy and computational efficiency of the real-time FE model.**

***Index Terms*—Electromagnetic transients, field-programmable gate arrays, field-circuit coupling, finite element method, parallel processing, power transformer, real-time systems, transmission line modeling.**

I. Introduction

TRANSFORMERS are essential components in a power delivery system. The behavior of the electromagnetic field in a transformer is governed by Ampere's law, and the accurate prediction of the magnetodynamic field is commonly obtained from the FEM simulation, a powerful numerical method to deal with complex geometries and material nonlinearities.

An accurate real-time electromagnetic *field-transient* simulation of a power transformer is of great benefit for the design and testing of better control and protection schemes, cost reductions, and energy efficiency improvement. However, as the permeability of the material depends on the magnetic field strength, solving the discretized nonlinear system of field equations in *space-time* requires iterative techniques such as the Newton-Raphson algorithm within each simulation time-step. Thus, a new linear system has to be solved at each iteration due to the updated Jacobian matrix, and the dense computation makes the traditional FEM solver unbearably slow for real-time execution. In the authors' knowledge, real-time simulation is only possible by simplifying the field problem to a lumped network. The traditional lumped models [1]–[6] used for electromagnetic transient simulation of the transformer include the admittance matrix based model and the topology-based magnetic equivalent circuit (MEC) model, both of which have been adequately utilized in real-time simulation [7], [8] for modeling various multi-winding transformers; nonlinear effects such as hysteresis and eddy current behavior have also been sufficiently represented. Although these analytical circuit-oriented models can be calculated fast, they suffer from oversimplification and serious information loss.

The transmission line modeling method is based on Huygens's principle and was originally developed by Johns [9] to simulate wave propagation. Then the concepts of TLM *link* and *stub* were proposed for the analysis of nonlinear networks to effectively decouple the nonlinear elements from the linear system [10]–[14]. Later Lobry and Deblecker insightfully uncovered the analogy between the finite element matrix and the nodal admittance matrix of a corresponding equivalent network and successfully applied the TLM technique to the FEM solution [15]–[17]. The improved computational efficiency and accuracy were notably discussed.

Solid foundations have been laid by previous scholars, yet the TLM technique used in FEM can be further explored for implementation on parallel hardware architectures to achieve the most computational efficiency, especially for real-time computation. In addition, the TLM-FE models in [15]–[17] are all fed with current sources, and an appropriate field-circuit coupling technique is necessary to interface with the external network.

A single TLM iteration is composed of two phases: *scattering* and *gathering*. In the scattering phase, pulses are injected from the linear network to each external element. Thus, all elements are decoupled from the network and the reflected pulses of external elements can be computed individually, i.e., the scattering phase can be perfectly parallelized. In the gathering phase, the reflected pulses return and impact on the linear network. Since the admittance matrix is determined by the impedance of the TLM links and remains unchanged, only one inversion is enough in the beginning. Thus, the computation of the gathering phase includes mainly matrix-vector multiplications with a changing right-hand side vector, which is also perfectly suitable for

Manuscript received September 21, 2017; revised December 26, 2017 and March 2, 2018; accepted March 3, 2018. Date of publication March 6, 2018; date of current version May 9, 2018. This work was supported by the Natural Science and Engineering Research Council of Canada. The work of P. Liu was supported by the China Scholarship Council (Funding No. 201506120058). Paper no. TPWRD-01179-2017. *(Corresponding author: Peng Liu.)*

The authors are with the Department of Electrical and Computer Engineering, University of Alberta, Edmonton, AB T6G 2R3, Canada (e-mail: pliu3@ualberta.ca; dinavahi@ualberta.ca).

Color versions of one or more of the figures in this paper are available online at http://ieeexplore.ieee.org.

Digital Object Identifier 10.1109/TPWRD.2018.2812753

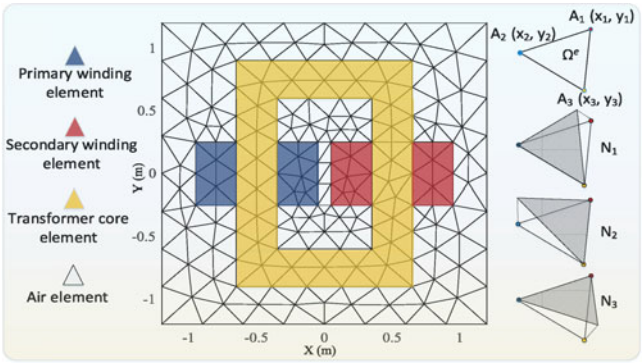

Fig. 1. 2-D FE model of a single-phase transformer.

parallel hardware architectures. In general, multiple TLM iterations are needed due to the mismatch between the impedance of the TLM link and the impedance of the element (linear or nonlinear). To decrease the number of TLM iterations required within each time-step, the impedances of the TLM links in this work are set to the memory steady-state values of the corresponding element instead of using arbitrary values.

In addition, an indirect non-iterative field-circuit coupling technique is proposed to handle the external network. The self and mutual inductances of the transformer windings are calculated based on the magnetic vector potentials from the FE model, and these coupling coefficients are fed to the external network, which is then solved independently within each time-step.

In this paper, the parallelism of the TLM-FE solution is fully explored to achieve real-time finite-element simulation of the electromagnetic transients in a 2D single-phase power transformer coupled to external networks. The real-time simulation is performed on the Virtex UltraScale+ VCU118 FPGA board, and the results are compared with those obtained from commercial FEM software Comsol Multiphysics with regard to accuracy and computational efficiency.

The paper is organized as the following. Section II presents the magnetodynamic field equations to be solved for the transformer, the TLM solution technique, and the field-circuit interface. In Section III, the detailed real-time implementation of the parallelized TLM technique on the FPGA is presented. Section IV provides the real-time simulation results and the comparisons. At last, Section V gives the conclusion.

II. Magnetodynamic Problem Formulation for Transformer FEM Simulation

A. FEM Equations

Consider a 2-D finite element model of a single-phase power transformer shown in Fig. 1. When the windings are excited by the external network, the current density in the windings produces a dynamic magnetic field, which is described by the magnetic vector potential A. Since the magnetic vector potential A and the impressed current density J only have the z-components in a 2-D problem, the nonlinear magnetodynamic problem can be defined by the following diffusion equation:

$$\nabla \cdot (\upsilon \nabla A) = \sigma \frac{\partial A}{\partial t} - J_z, \tag{1}$$

where υ is the field-dependent reluctivity; σ is the conductivity, a constant value for a certain material; J_z is the impressed current density, which is only nonzero in the winding zone.

The well-known Galerkin FEM [18] applied to solve the magnetodynamic problem includes the following steps: discretize the domain, form elemental equations, assemble the global matrix, and solve the system of equations.

Fig. 1 shows the discretized domain consisting of triangular elements and nodes. For the Galerkin method, the product of the residual and the weighted function is integrated over each element, and the element equations can be formed by forcing the integral to zero. With natural boundary conditions applied, the classical weighted-integral equation of element Ω^e can be written as:

$$\iint_{\Omega^e} \upsilon^e \left(\frac{\partial A^e}{\partial x}\frac{\partial W^e}{\partial x} + \frac{\partial A^e}{\partial y}\frac{\partial W^e}{\partial y} \right) dxdy + \iint_{\Omega^e} \sigma \frac{\partial A^e}{\partial t} W^e dxdy = \iint_{\Omega^e} J_z^e W^e dxdy, \tag{2}$$

where A^e is the magnetic vector potential over element Ω^e, and W^e the weighted function. In Fig. 1, the vertex values of the triangular element Ω^e are A_1, A_2, and A_3, and the magnetic vector potential over the whole element A^e can be expressed with the classical barycentric interpolation:

$$A^e = N_1 A_1 + N_2 A_2 + N_3 A_3, \tag{3}$$

where N_1, N_2, and N_3 are the shape functions profiled in Fig. 1. The values of these shape functions at any position $(x,\ y)$ are defined by

$$N_i = \frac{1}{2\Delta^e}(a_i + b_i x + c_i y)(i = 1,\ 2,\ 3), \tag{4}$$

where Δ^e is the area of the triangular element; a_i, b_i, and c_i are related to the coordinates of the vertices:

$$\begin{aligned} &a_1 = x_2y_3 - x_3y_2,\ b_1 = y_2 - y_3,\ c_1 = x_3 - x_2,\\ &a_2 = x_3y_1 - x_1y_3,\ b_2 = y_3 - y_1,\ c_2 = x_1 - x_3,\\ &a_3 = x_1y_2 - x_2y_1,\ b_3 = y_1 - y_2,\ c_3 = x_2 - x_1. \end{aligned} \tag{5}$$

According to the Galerkin method, the A^e in (2) is substituted by (3) and the weighted functions W^e are set to N_1, N_2, and N_3 respectively. Thus, 3 equations with 3 unknown vertex magnetic potential values are obtained after accomplishing the integral:

$$\frac{\upsilon^e}{4\Delta^e}\begin{bmatrix} b_1b_1 + c_1c_1 & b_1b_2 + c_1c_2 & b_1b_3 + c_1c_3 \\ b_1b_2 + c_1c_2 & b_2b_2 + c_2c_2 & b_2b_3 + c_2c_3 \\ b_1b_3 + c_1c_3 & b_2b_3 + c_2c_3 & b_3b_3 + c_3c_3 \end{bmatrix}\begin{bmatrix} A_1 \\ A_2 \\ A_3 \end{bmatrix} + \frac{\sigma^e\Delta^e}{12}\begin{bmatrix} 2 & 1 & 1 \\ 1 & 2 & 1 \\ 1 & 1 & 2 \end{bmatrix}\begin{bmatrix} \frac{\partial A_1}{\partial t} \\ \frac{\partial A_2}{\partial t} \\ \frac{\partial A_3}{\partial t} \end{bmatrix} = \frac{J_z^e\Delta^e}{3}\begin{bmatrix} 1 \\ 1 \\ 1 \end{bmatrix}. \tag{6}$$

Note that the reluctivity υ^e, the conductivity σ^e and the current density J_z^e are constant over one finite element. The distributions of σ^e and J_z^e are given while υ^e depends on A_1, A_2, and A_3. The dependence is not straightforward and could be quantitatively expressed by introducing the magnetic flux density B. In a 2-D problem, as A is defined by $B = \nabla \times A$, in one element B and

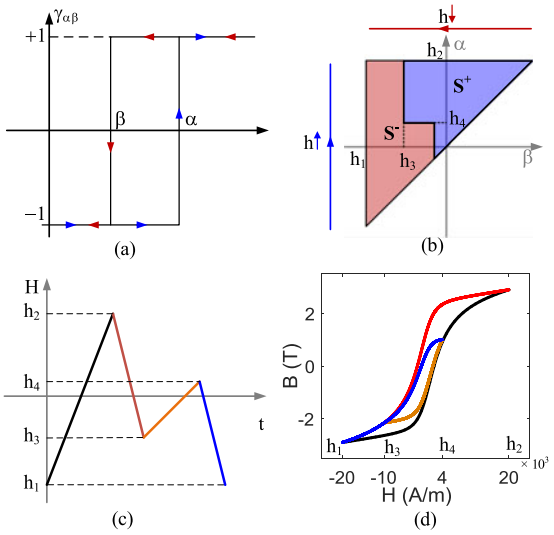

Fig. 2. Preisach model: (a) hysteresis operator, (b) Preisach triangle, (c) sample input of H, and (d) trajectory of the hysteresis loop.

A are related by:

$$B^2 = \left(\frac{\partial A^e}{\partial x}\right)^2 + \left(\frac{\partial A^e}{\partial y}\right)^2 = -\frac{1}{4(\Delta^e)^2}((b_1b_2 + c_1c_2)(A_1 - A_2)^2 + (b_2b_3 + c_2c_3)(A_2 - A_3)^2 + (b_1b_3 + c_1c_3)(A_1 - A_3)^2). \quad (7)$$

The $\upsilon^e - B^2$ relationship can be found from the core material property such as the B-H curve representation. In this paper, the nonlinear material property of the transformer core is represented using the Preisach model [19].

The classical Preisach model regards the ferromagnetic material as an infinite set of hysterons defined by the hysteresis operator (Fig. 2(a)). Thus the magnetization moment M can be written as the following integral over the Preisach triangle (Fig. 2(b)):

$$M(t) = \iint_{\alpha \geq \beta} \mu(\alpha, \beta)\gamma_{\alpha\beta}H(t)d\alpha d\beta = \iint_{S^+} \mu(\alpha, \beta)H(t)d\alpha d\beta - \iint_{S^-} \mu(\alpha, \beta)H(t)d\alpha d\beta, \quad (8)$$

where $H(t)$ and $M(t)$ are the input and output, the stair-shaped boundary of S^+ and S^- is determined by the historical extremum of $H(t)$, and $\mu(\alpha, \beta)$ is the Preisach distribution function that is usually obtained from the experimental results. Thus the B-H relationship can be obtained:

$$B = \mu_0(M + H). \quad (9)$$

For the Newton-Raphson algorithm requiring smooth nonlinearity, it is beneficial to approximate the experimental results using an mathematical distribution function. According to [20], the following 2-D Cauchy distribution function, which is analytically integrable, can achieve an accurate approximation:

$$\mu(\alpha, \beta) = c\frac{1}{1 + \left(\frac{\alpha - a_0}{b0}\right)^2}\frac{1}{1 + \left(\frac{\beta - a_1}{b1}\right)^2}, \quad (10)$$

where a_0, a_1, b_0, b_1, and c are coefficients given in the appendix.

Since the magnetization moment M depends on the past history of H, a reversal point vector (RPV) storing the historical extremum (h_1, h_2, h_3, h_4, ...) is required to derive the integral. Fig. 2(c) and (d) present a sample input with 4 branches and the corresponding trajectories of the hysteresis loop. The RPV is updated or wiped out (branch $h_4 \rightarrow h_1$) based on the input sequence $H(t)$, and the B-H formulation in different branches are regulated by the RPV.

The problem domain is enclosed by an artificial rectangular boundary Γ (shown in Fig. 1), and the boundary condition is $A_\Gamma = 0$. After time discretization, the above nonlinear elemental equations (6) can be assembled and are ready to be solved with the Newton-Raphson iterative scheme. With respect to the computational burden, the TLM technique provides an efficient methodology to handle these nonlinear equations.

B. Refined TLM Solution

When the TLM technique is applied to solve an electrical circuit in the time domain, the components are separated from the network by lossless transmission lines. The characteristic impedance of the transmission line Z_c is arbitrary for resistors, $\Delta t/2C$ for capacitors, and $2L/\Delta t$ for inductors, where Δt is the simulation time-step.

In the scattering phase, the network transmits incident impulses V_i into each element. For linear elements, the reflected pulse can be calculated by

$$V_r = K_r V_i, \quad (11)$$

where the reflection coefficient K_r is equal to $(R - Z_c)/(R + Z_c)$ for resistors, 1 for capacitors, and -1 for inductors. For a nonlinear element, for example, a nonlinear resistor described as $U = f(I)$, the reflected pulse V_r is obtained by solving the nonlinear equation

$$V_i + V_r = f\left(\frac{V_i - V_r}{Z_c}\right). \quad (12)$$

Note that if Z_c is equal to the working state value of the linear or nonlinear resistor, the reflection coefficient is 0 and only one TLM iteration is required.

In the gathering phase, all the reflected pulses return to the network and update the values of all nodes. The transmission line and the elements are replaced with their equivalent Norton circuits.

The nodal values can be updated by solving a linear network with unchanged nodal admittance matrix, then the next incident pulse can be also updated by:

$$V_i = V_d - V_r, \quad (13)$$

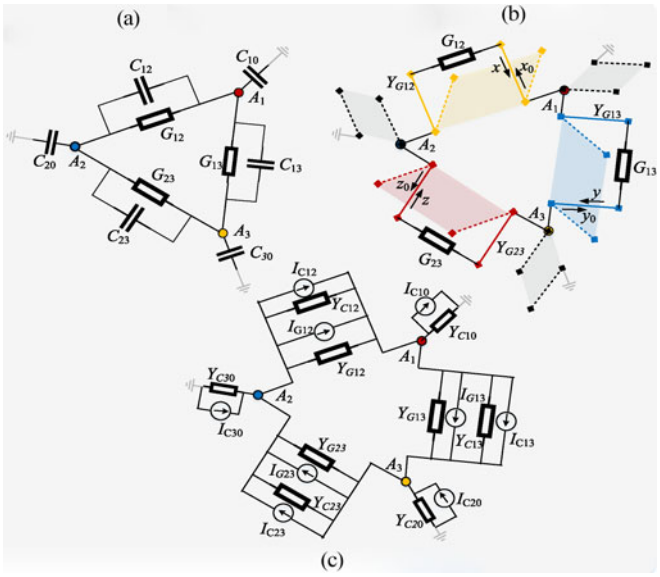

Fig. 3. TLM technique applied to elemental equations of the FEM.

where V_d is the nodal voltage difference. Thus, the gathering phase is complete, and the scattering phase of the next TLM iteration is ready to begin.

Equation (6) defines an equivalent network composed of capacitors and nonlinear resistors shown in Fig. 3(a). The magnetic vector potential is modeled as the electric potential, the right-hand side vector of (6) is modeled as the current sources and the Dirichlet boundary conditions are modeled as the voltage sources. The nonlinear resistors and the linear capacitors form the coefficient matrix and hold such material properties as reluctivity and conductivity. And the values of the components are given as

$$G_{12} = -\frac{\upsilon^e}{4\Delta^e}(b_1b_2 + c_1c_2),\quad Y_{G12} = -\frac{\upsilon_g^e}{4\Delta^e}(b_1b_2 + c_1c_2),$$
$$G_{13} = -\frac{\upsilon^e}{4\Delta^e}(b_1b_3 + c_1c_3),\quad Y_{G13} = -\frac{\upsilon_g^e}{4\Delta^e}(b_1b_3 + c_1c_3),$$
$$G_{23} = -\frac{\upsilon^e}{4\Delta^e}(b_2b_3 + c_2c_3),\quad Y_{G23} = -\frac{\upsilon_g^e}{4\Delta^e}(b_2b_3 + c_2c_3),$$
$$C_{12} = C_{13} = C_{23} = -\frac{\sigma^e\Delta^e}{12},$$
$$Y_{C12} = Y_{C13} = Y_{C23} = -\frac{\sigma^e\Delta^e}{6\Delta t},$$
$$C_{10} = C_{20} = C_{30} = \frac{4\sigma^e\Delta^e}{12},$$
$$Y_{C10} = Y_{C20} = Y_{C30} = \frac{4\sigma^e\Delta^e}{6\Delta t}. \tag{14}$$

where υ^e is the prior unknown reluctivity to be solved using the 3×3 Newton-Raphson scheme and υ_g^e is an initial guess value, which should be as close to υ^e as possible. With the guessed υ_g^e, the nodal admittance matrix required in the gathering phase could be obtained by assembling multiple Norton equivalent circuits (Fig. 3(c)) based on the FE mesh information.

When the TLM technique is applied in a triangular network, three pulses based on the differences between nodal values will be injected into the three edges. Fig. 3(b) shows the TLM links (resistors) and the TLM stubs (capacitors) in the scattering phase. The incident pulses into three edges are denoted by $x_0,\ y_0$, and z_0 and the reflected pulses to be calculated are denoted by $x,\ y$, and z, respectively. Instead of solving a single equation (12), the following three coupled nonlinear algebraic equations need to be solved:

$$G_{12}(x + x_0) - Y_{G12}(x_0 - x) = 0,$$
$$G_{13}(y + y_0) - Y_{G13}(y_0 - y) = 0,$$
$$G_{23}(z + z_0) - Y_{G23}(z_0 - z) = 0. \tag{15}$$

Since $G_{12},\ G_{13}$ and G_{23} are functions of $(x + x_0)$, $(y + y_0)$ and $(z + z_0)$, and the relations can be derived from (7) and the Preisach model, the resulting nonlinear algebraic equations can be efficiently solved with the Newton-Raphson method, and the convergence can be sped up using an appropriate relaxation factor. When calculating the 3×3 Jacobian matrix, the following chain rule is utilized:

$$\frac{\partial G}{\partial x} = \frac{\partial G}{\partial B^2}\frac{\partial B^2}{\partial x}. \tag{16}$$

In the gathering phase shown in Fig. 3(c), the reflected pulses and the TLM links or stubs are replaced with their equivalent Norton circuits. It is a linear network and the nodal values can be updated after matrix-vector multiplications if the inversion of the admittance matrix is ready at the beginning.

It should be emphasized that the above descriptions of the TLM technique applied in FEM are at the triangular element level. For a problem domain composed of numerous finite elements, the main computational tasks include solving (15) for all nonlinear elements in the scattering phase and the matrix-vector multiplications in the gathering phase. Both tasks could be perfectly parallelized on massively parallel computing architectures.

It is acknowledged that multiple TLM iterations are needed because of the mismatch of the unknown υ^e and the guessed υ_g^e. If υ^e is equal to υ_g^e, the reflected pulse is zero and only one TLM iteration is enough for convergence. Fewer TLM iterations are needed if the two values are closer. Thus, the concept of *memory* nodal admittance matrix is proposed to decrease the mismatch and to accelerate the convergence. A memory admittance matrix is featured by the impressed current density. For the transformer, once the FE model is solved with provided I_{p0} and I_{s0}, the υ^e of each element can be extracted. After the assembly and inversion process, these values could be utilized to form a new admittance matrix, which contains very valuable information (memory) for the rest solution.

Fig. 4(a) shows the efficiency of the memory admittance matrix in a case study (presented in Section IV) with secondary winding open-circuited ($I_s = 0$). As shown in the figure, even when the υ_g^e is carefully guessed, it takes more than 30 TLM iterations for each time-step while the number is around 10 utilizing the memory admittance matrix. Note that $I_p^{\max}$ in Fig. 4(a) could be set to the peak value of the rated primary winding current.

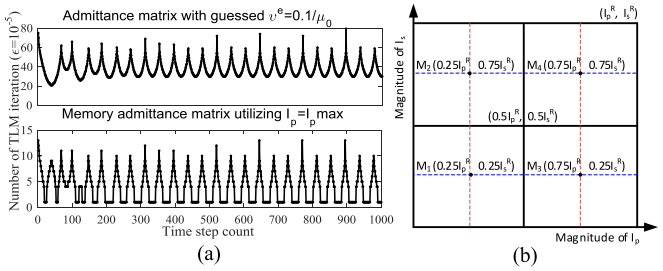

Fig. 4. (a) TLM iteration number required utilizing guessed and memory admittance matrix. (b) Four memory matrices formation and usage.

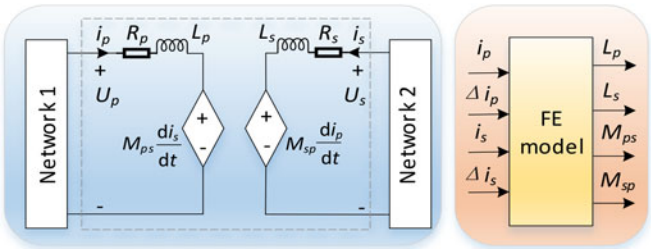

Fig. 5. Equivalent FE transformer model coupled to external networks.

In this work, a total of four memory admittance matrices are applied to ensure that the TLM iteration number is always less than 5 provided that I_p and I_s change arbitrarily within each time-step, as shown in Fig. 4(b), where I_p^R and I_s^R are the rated currents in the primary and secondary windings of the transformer. Different admittance matrices are used for the gathering phase based on the combination of the I_p and I_s. The decreased TLM iteration number and the parallelism within a TLM iteration make real-time simulation possible on the parallel FPGA hardware architecture.

C. Field-Circuit Coupling

Note that the inputs of the FE model described above are the winding currents. However, since a transformer is generally excited by voltage sources in a power system, a field-circuit coupling technique is necessary to interface with the external circuit.

Direct coupling and indirect coupling approaches have been explored to interface the FE model and the external network: the direct coupling approach solves the field equations and the electrical network equations simultaneously while the indirect approach solve the two subsystems separately [21]. The computational burden of the direct coupling approach is heavier than the traditional FEM solver because the circuit equations destroy the matrix symmetry [22].

In this paper, we proposed an indirect coupling technique by accurately extracting the self and the mutual inductances of the transformer from the FE model. Within each time-step, the field equations and the circuit equations are solved separately without having to apply any iterative scheme.

In electrical networks, a transformer model can be represented by self and mutual inductances with controlled sources, as shown in Fig. 5. The accurate values of these nonlinear inductances (depends on the winding currents) can be obtained with the FE model. In fact, the electric voltage U across a winding can be represented by the magnetic vector potential and the voltage drop of winding's resistance:

$$U = rI + \frac{Nl}{\Delta_S}\int_S \frac{\partial A}{\partial t} dS, \tag{17}$$

where I is the winding current, r the winding resistance, N the number of turns, l the axial length of each filament, S the winding zone, and Δ_S the area of the winding zone.

Since A is a function of the primary winding current i_p and the secondary winding current i_s based on the FE model, (17) can be rewritten as:

$$U = rI + \frac{Nl}{\Delta_S}\int_S \frac{\partial A}{\partial i_p} dS \frac{\partial i_p}{\partial t} + \frac{Nl}{\Delta_S}\int_S \frac{\partial A}{\partial i_s} dS \frac{\partial i_s}{\partial t}. \tag{18}$$

Applying (18) to the primary and the secondary winding respectively, the self and mutual inductances of the transformer can be obtained as:

$$L_p = \frac{N_p l_p}{\Delta_{S_p}}\int_{S_p} \frac{\partial A}{\partial i_p} dS,\ M_{ps} = \frac{N_p l_p}{\Delta_{S_p}}\int_{S_p} \frac{\partial A}{\partial i_s} dS,$$
$$M_{sp} = \frac{N_s l_s}{\Delta_{S_s}}\int_{S_s} \frac{\partial A}{\partial i_p} dS,\ L_s = \frac{N_s l_s}{\Delta_{S_s}}\int_{S_s} \frac{\partial A}{\partial i_s} dS. \tag{19}$$

Since

$$\frac{\partial A}{\partial i_p} = \frac{A(i_p + \Delta i_p, i_s) - A(i_p, i_s)}{\Delta i_p},$$
$$\frac{\partial A}{\partial i_s} = \frac{A(i_p, i_s + \Delta i_s) - A(i_p, i_s)}{\Delta i_s}, \tag{20}$$

these coupling coefficients can be calculated with the FE model by setting the Δi_p and Δi_s in (20) to a very small value such as 0.1 A.

It is known that by applying Trapezoidal rule, a constant inductor in the network can be replaced by a resistor $\frac{2L(t)}{\Delta t}$ in parallel with a current source I_{his}. When the inductor value $L(t)$ is time-varying, both $L(t)$ and $L(t+\Delta t)$ should be used. Since $L(t+\Delta t)$ is unknown, an error exists in the proposed indirect coupling scheme because the time-varying inductances at time point t, calculated from $i_p(t)$ and $i_s(t)$, are utilized to solve the external networks at time point $t+\Delta t$. To reduce the asynchronization error, the inductance values at time point $t+\frac{\Delta t}{2}$ are used with a prediction scheme and the following central difference formula is utilized:

$$\frac{\partial A}{\partial i_p}\left(t+\frac{\Delta t}{2}\right) \approx \frac{A(i_p(t+\Delta t), i_s(t)) - A(i_p(t), i_s(t))}{i_p(t+\Delta t) - i_p(t)},$$
$$\frac{\partial A}{\partial i_s}\left(t+\frac{\Delta t}{2}\right) \approx \frac{A(i_p(t), i_s(t+\Delta t)) - A(i_p(t), i_s(t))}{i_s(t+\Delta t) - i_s(t)}. \tag{21}$$

where $i_p(t+\Delta t)$ and $i_s(t+\Delta t)$ are unknown and can be predicted from their historical values:

$$i_p(t+\Delta t) = 2i_p(t) - i_p(t-\Delta t),$$
$$i_s(t+\Delta t) = 2i_s(t) - i_s(t-\Delta t). \tag{22}$$

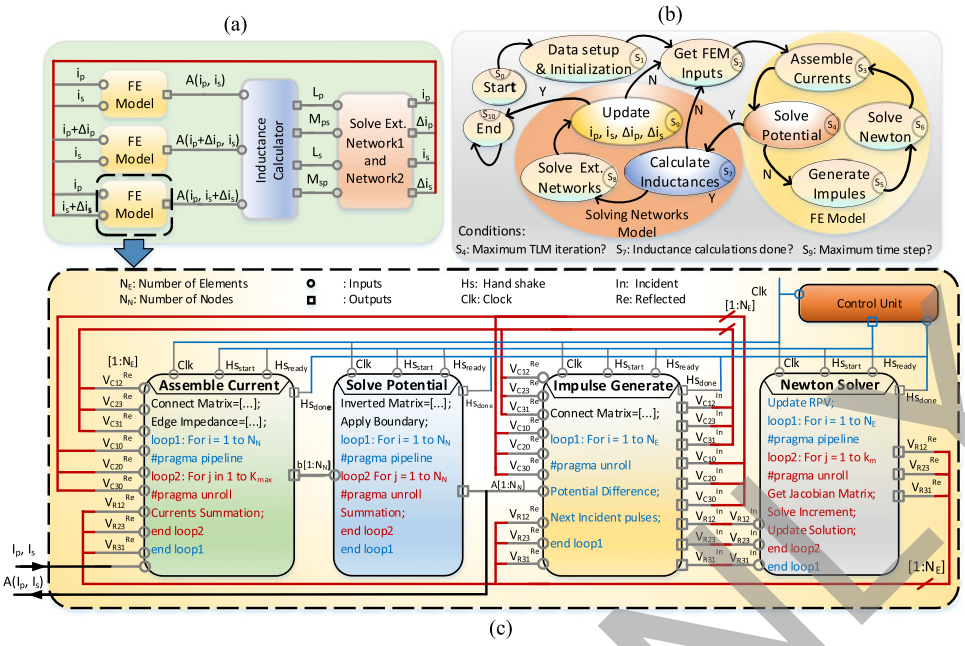

Fig. 6. Real-time hardware emulation of the finite-element computation for the transformer on FPGA.

Simulation results show that the mean absolute relative error is less than 3% with $\Delta i_p = i_p(t) - i_p(t-\Delta t)$, $\Delta i_s = i_s(t) - i_s(t-\Delta t)$ and more than 5% using small values (0.1 A) of Δi_p and Δi_s.

Note that the calculation of $A(i_p, i_s)$, $A(i_p, i_s + \Delta i_s)$, and $A(i_p + \Delta i_p, i_s)$ can be also parallelized with enough hardware resources. Then, these parameters are fed to the external electrical network for simulation using the electromagnetic transients program (EMTP) approach [23].

III. Real-Time Hardware Emulation of the Transformer Finite Element Model

The hardware design was implemented on the Xilinx Virtex UltraScale+ VCU118 board with the xcvu9p-flga2104-e-es1 FPGA using high-level synthesis and optimization. The sequential C and C++ functions can be compiled down to hardware IP blocks with inputs, outputs, and handshake signals for interfacing, which can be optimized based on user's preferences by adding the directives such as array partitioning, loop unrolling, and pipelining, as shown in (23) at the bottom of the page.

According to the TLM-FE solution and the field-circuit coupling technique, six hardware blocks are generated and optimized to achieve deep data pipelining on the FPGA. The detailed real-time implementation on the FPGA is shown in Fig. 6. The block connections, pseudo codes, and the finite state machine are all illustrated. The functionalities of these blocks are presented as the following:

1) *Assemble Current:* The currents generated by the reflected pulses in each triangular element (Fig. 3) and the impressed source currents are assembled to obtain the total current injected to each node. The assembly of each node is parallelized and pipelined based on the node-element connection matrix.
2) *Solve Potential:* With the assembled current vector and the inverted nodal admittance matrix, the magnetic potential of each node is calculated by the matrix-vector multiplication under the Dirichlet boundary conditions. The multiplications could be totally parallelized and the summation could be accomplished using a tree adder with a latency of $O(\log_2 N)$.
3) *Impulse Generator:* Based on the updated magnetic vector potential and the reflected pulses, the new incident pulses are generated for each triangular element. For each element, these operations are unrolled and executed in parallel.
4) *Newton Solver:* For each triangular element, the 3 incident pulses are taken as inputs to obtain the 3 reflected pulses. The Newton solver is also unrolled and fully pipelined to treat multiple elements. In this work, by using a relaxation factor of 1.2, 6 iterations are enough for all elements to maintain a relative tolerance of 10^{-5}.

$$\begin{bmatrix} \frac{2(L_p+L_1)}{\Delta t} + R_1 + R_p & -\frac{2M_{ps}}{\Delta t} & 0 \\ \frac{2M_{sp}}{\Delta t} & -R_s - \frac{2L_s}{\Delta t} - Z_{TL} & 0 \\ 0 & 0 & R_{L2} + \frac{2L_{L2}}{\Delta t} + Z_{TL} \end{bmatrix} \begin{bmatrix} I_p(t+\Delta t) \\ I_s(t+\Delta t) \\ I_k(t+\Delta t) \end{bmatrix} = \begin{bmatrix} \frac{2(L_p+L_1)}{\Delta t} I_p^{his} - \frac{2M_{ps}}{\Delta t} I_s^{his} + V_{ac}(t+\Delta t) \\ \frac{2M_{sp}}{\Delta t} I_p^{his} - \frac{2L_s}{\Delta t} I_s^{his} - U_k(t) + Z_{TL} I_k(t) \\ \frac{2L_{L2}}{\Delta t} I_k^{his} + U_s(t) - Z_{TL} I_s(t) \end{bmatrix}. \tag{23}$$

TABLE I
HARDWARE RESOURCE UTILIZATION AND TIMING REPORT

FPGA device	Module	Resource utilization				Latency (clock cycles)
		BRAM	DSP	FF	LUT	
Xilinx UltraScale+ xcvu9p	Assem. curr.	84	512	130316	253004	393
	Solv. poten.	168	842	86841	64301	206
	Imp. gener.	0	24	4418	21316	157
	Newt. solv.	9	1646	194969	200509	767
	Subtotal (FEM)	6%	44.2%	17.6%	45.6%	1523
	Calc. induc.	0	33	4971	5237	71
	Solve netw.	0	5	1611	1758	82
	Subtotal (Netw.)	0%	1%	0%	0%	153
Xilinx UltraScale+ xcvu13p	Assem. curr.	84	512	131490	257507	399
	Solv. poten.	168	842	86876	64805	208
	Imp. gener.	0	24	5187	21524	159
	Newt. solv.	9	1646	214112	203558	770
	Subtotal (FEM)	4.9%	24.6%	12.7%	31.7%	1536
	Calc. induc.	0	33	4991	5287	72
	Solve netw.	0	5	1811	1958	84
	Subtotal (Netw.)	0%	1%	0%	0%	156

5) *Inductance Calculator:* Once $A(i_p, i_s)$, $A(i_p, i_s + \Delta i_s)$, and $A(i_p + \Delta i_p, i_s)$ are available, the self and mutual inductances can be calculated by the integration in (19).
6) *Solve External Networks:* The transformer is converted to the equivalent model in Fig. 5 with all inductances known, and the external electrical networks are solved in the time-domain. For example, in Case Study II, when the Bergeron transmission line is loaded, the KVL equations to be solved are given in (23). Note that although the execution time of the external network solution is slight compared with the FE model, the 3×3 matrix in (23) is also time-varying due to the time-varying transformer inductances. For larger external networks, the compensation method could be applied to handle these time-varying nonlinear transformer inductances [7].

Table I shows the FPGA hardware utilization and the timing report of the case study with a FE model composed of 196 nodes and 358 elements, which are compiled on both Xilinx Virtex UltraScale+ xcvu9p and xcvu13p FPGAs, and the details of the case study are presented in the next section.

Although the FPGA clock frequency of each hardware block can reach more than 115 MHz, the maximum clock frequency of the design can reach 93.1 MHz for xcvu9p and 94.2 MHz for xcvu13p after the hardware blocks are interconnected. Since 5 TLM iterations are required for a reasonable accuracy, according to the timing report, the execution time of the FE hardware block is $5 \times 1523 \div 93.1 = 81.8$ μs on the xcvu9p FPGA and $5 \times 1536 \div 94.2 = 81.6$ μs on xcvu13p while the latency of the circuit model is 1.7 μs. According to the hardware utilization report, two FE hardware blocks can be generated on the xcvu9p FPGA and three FE hardware blocks on the xcvu13p FPGA. Therefore, for the design on the xcvu9p FPGA, two of $A(i_p, i_s)$, $A(i_p, i_s + \Delta i_s)$, and $A(i_p + \Delta i_p, i_s)$ can be calculated in parallel and the remaining one is executed sequentially thereafter, and the total execution time of the implementation is therefore 166 μs. For the xcvu13p FPGA, the calculations of $A(i_p, i_s)$, $A(i_p, i_s + \Delta i_s)$, and $A(i_p + \Delta i_p, i_s)$ can all be executed in parallel at the same time and the total execution time of the implementation is 84 μs.

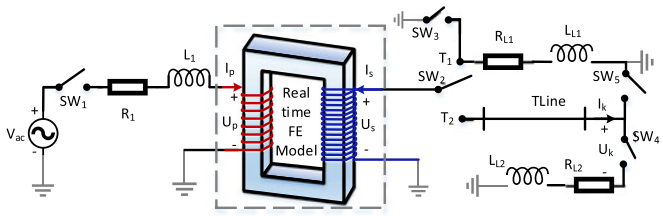

Fig. 7. Schematic of the transformer FE model coupled with external networks for case studies.

Although an execution time of 166 μs of the design on UltraScale+ xcvu9p FPGA in our real-time implementation is still too large for the electromagnetic transients requiring a time-step of 50 μs, it should be pointed out that the proposed indirect coupling scheme works perfectly for multi-rate real-time simulation, which means that the external networks can utilize a much smaller time-step than that of the FE model. For example, in Case Study II presented in Section IV, the time-step is 180 μs for the FE transformer model and 45 μs for the external networks, implying that the transformer inductances used in the solution of the external network module are updated every 4 time-steps. In our future work implemented on the UltraScale+ xcvu13p FPGA, the applied simulation time-step for the FE model could be 84 μs.

IV. CASE STUDIES AND RESULTS

A. Setup for Case Study

A single-phase power transformer rated at 37.5 kV/202 kV was studied in this work, and the geometry and mesh (196 nodes and 358 elements) are shown in Fig. 1. The schematic of the real-time FE model coupled to external networks is shown in Fig. 7. The primary winding is excited by a 60 Hz AC voltage source, and a Bergeron line model is included between the secondary winding and the load. The detailed simulation parameters are provided in the appendix.

Two case studies: single-rate and multi-rate, are presented. For the Case Study I, the total simulation time is 600 ms and the applied time-step is 180 μs for the FE transformer model and the external networks. The following events are simulated:

1) t = 0, $\mathrm{SW_1}$ is turned on and the transformer is energized while the secondary winding is open-circuited.
2) t = 150 ms, $\mathrm{SW_2}$ is turned to $\mathrm{T_1}$ and the transformer works with a load of $\mathrm{R_{L1}}$ and $\mathrm{L_{L1}}$.
3) t = 300 ms, the second and the fourth harmonics are injected into the voltage source $\mathrm{V_{ac}}$.
4) t = 450 ms, $\mathrm{SW_3}$ is turned on and the secondary winding is short-circuited.

For the Case Study II, the total simulation time is 600 ms and the applied time-step is 180 μs for the FE transformer model and 45 μs for the external networks. The following events are simulated:

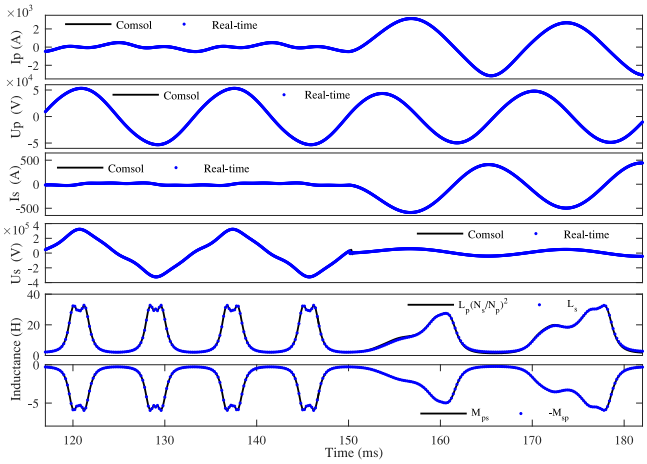

Fig. 8. Zoomed-in time-domain result comparison in Case Study II between 117 ms and 182 ms.

1) $t = 0$, SW_1 is turned on and SW_2 is turned to T_2, the transformer is connected to a transmission line with an open-circuited receiving end.
2) $t = 150$ ms, SW_4 is turned on and the the transmission line is loaded with R_{L2} and L_{L2}.
3) $t = 300$ ms, the second and the fourth harmonics are injected into the voltage source V_{ac}.
4) $t = 450$ ms, SW_5 is turned on and the transmission line is short-circuited.

B. Results and Validation

The off-line simulation with the same case study, setup and mesh was also performed on the commercial FEM software Comsol. Mesh dependency test has been performed in Comsol and it turned out that for this 2-D problem, 196 nodes are enough to maintain reasonable accuracy compared with a finer mesh. The off-line results are regarded reliable and are thus used as the benchmark for comparison for the real-time results. The real-time simulation results of the primary winding current I_p, the primary winding voltage U_p, the secondary winding current I_s, the secondary winding voltage U_s, the transformer inductances, the time-varying winding loss, eddy current loss, hysteresis loss and total loss are all presented in Fig. 11 for Case Study I and Fig. 12 for Case Study II, respectively, with a comparison of those results from Comsol. Note that all the errors in the figures denote the mean absolute relative error. The zoomed-in plot of the simulation results is shown in Fig. 8. For all practical purposes the real-time results are identical to the Comsol results, and the harmonics from Fast Fourier transform of the results also match.

As can be seen from the results, when the secondary winding is open-circuited, I_p is the magnetizing current and the phase difference of I_p and U_s is always 90°. The inrush current of the primary winding occurs at $t = t_1$ while the inrush current of the secondary winding occurs at $t = t_5$. The inrush currents may cause some unwanted phenomenon such as saturation in the transformer, which is possible to be monitored in real-time with the proposed implementation.

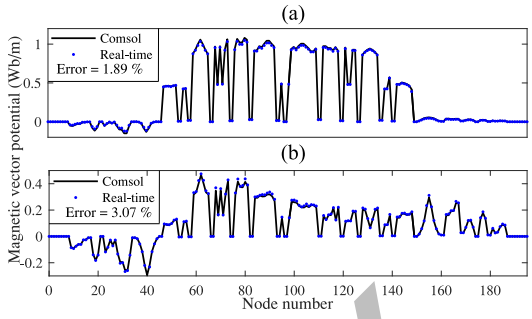

Fig. 9. Magnetic vector potential comparison at t_1 in Case Study I and at t_5 in Case Study II. (a) Case study I, $t = t_1$. (b) Case study II, $t = t_5$.

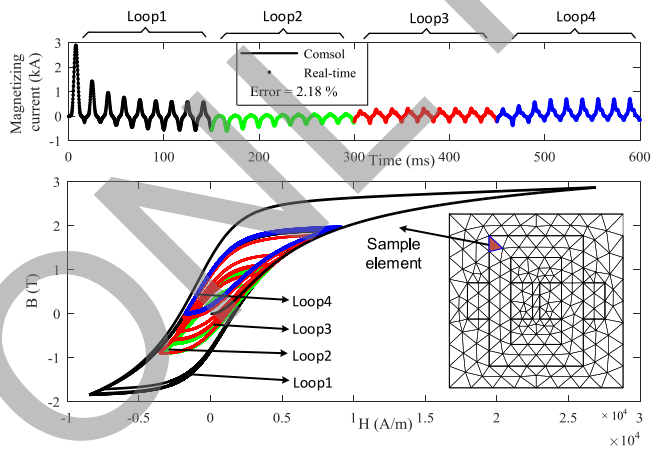

Fig. 10. Magnetizing current and the trajectories of the hysteresis loop of a sample triangular element in Case Study I.

The direct output of the FE model is the magnetic vector potential A, and Fig. 9 shows the node solution of the real-time implementation compared with the Comsol at $t = t_1$ in Case Study I and at $t = t_5$ in Case Study II.

Other variables can also be derived after post-processing. For example, the induced electric field E and the eddy current loss L_{ec} can be calculated with

$$E = \frac{\partial A}{\partial t}, \quad L_{ec} = \iint_{\Omega_{core}} \sigma^e E^2. \tag{24}$$

Fig. 10 shows the magnetizing current and the trajectories of the hysteresis loop in a sample element in Case Study I, and the hysteresis loss can be also calculated based on these loops, which are regulated by the RPV.

The detailed field distributions of the magnetic vector potential A (Wb/m), the magnetic flux density B (T), the magnetic field strength H (A/m), and the eddy current density J (A/m^2) at $t = t_1$ in Case Study I and at $t = t_5$ in Case Study II are also captured and presented in Figs. 12 and 13, respectively.

Note that the error in the case study is caused by two aspects: the FE-TLM solution and the non-iterative coupling scheme. It turned out that given the same I_p and I_s, the error of the magnetic vector potential from the real-time results is less than 0.1% compared with the Comsol solver. Further increasing the TLM iteration and the Newton iteration will make this error

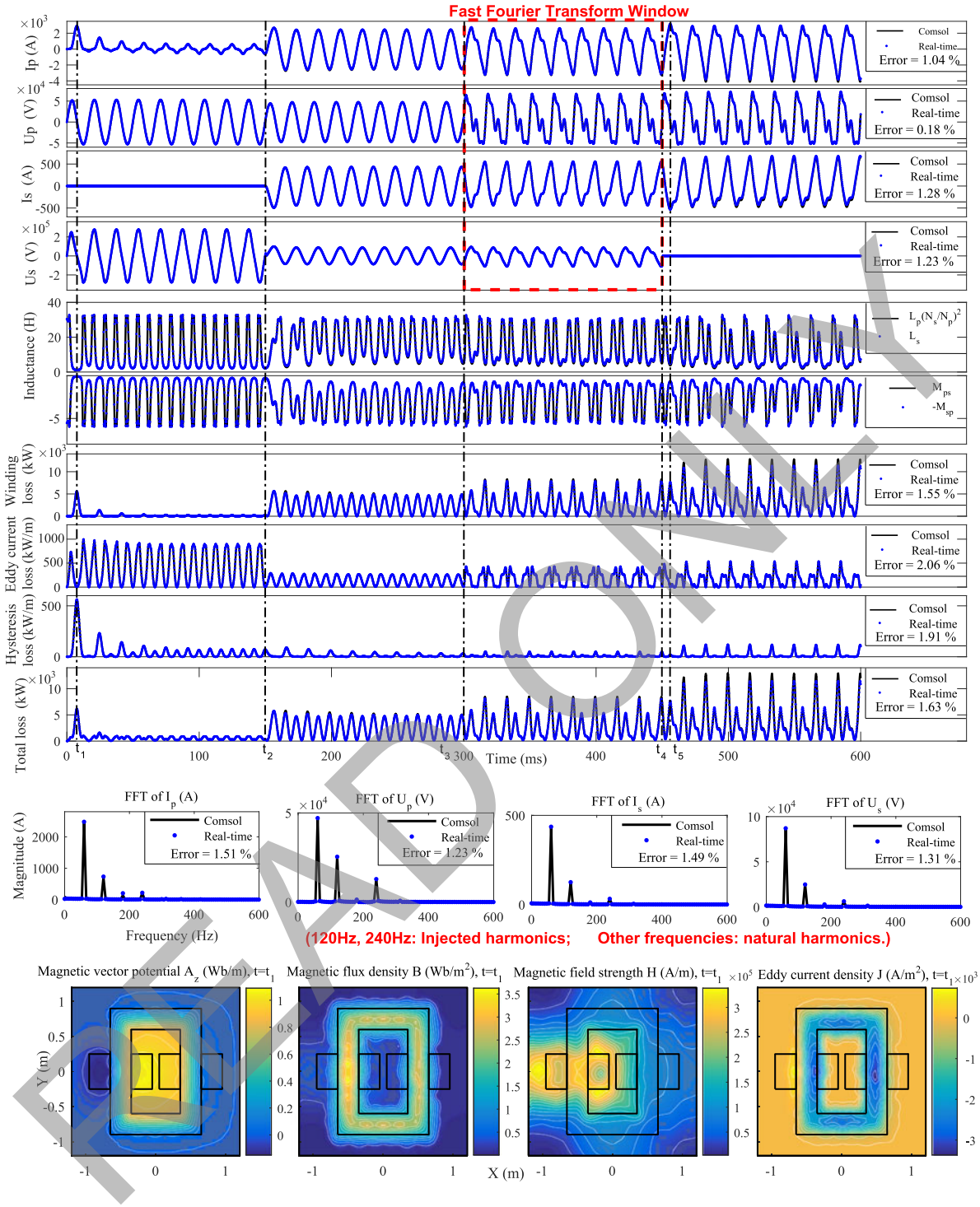

Fig. 11. Real-time simulation results and the comparison with Comsol off-line results for **single-rate** Case Study I: time-domain, frequency-domain, and field distributions.

smaller. Thus we believe the error in our work mainly come from the non-iterative coupling scheme.

C. Speed-Up and Scalability

The off-line simulation with Comsol was conducted on a PC with the CPU Intel Xeon E5-2620, 16 cores, 2.1 GHz clock frequency, and 32 GB RAM. The tolerance of the Comsol nonlinear solver is 10^{-5} and the maximum iteration number is set to 20. The order of the finite element is 1. It takes 134 s to run 3333 simulation time-steps, and the execution time per solution step is 40 ms. By sufficiently exploring the parallelism and deep data pipelining, the speed-up of the real-time hardware implementation can reach 241 times.

The proposed real-time approach also has good scalability. Although a simple circuit is used in the case study, the

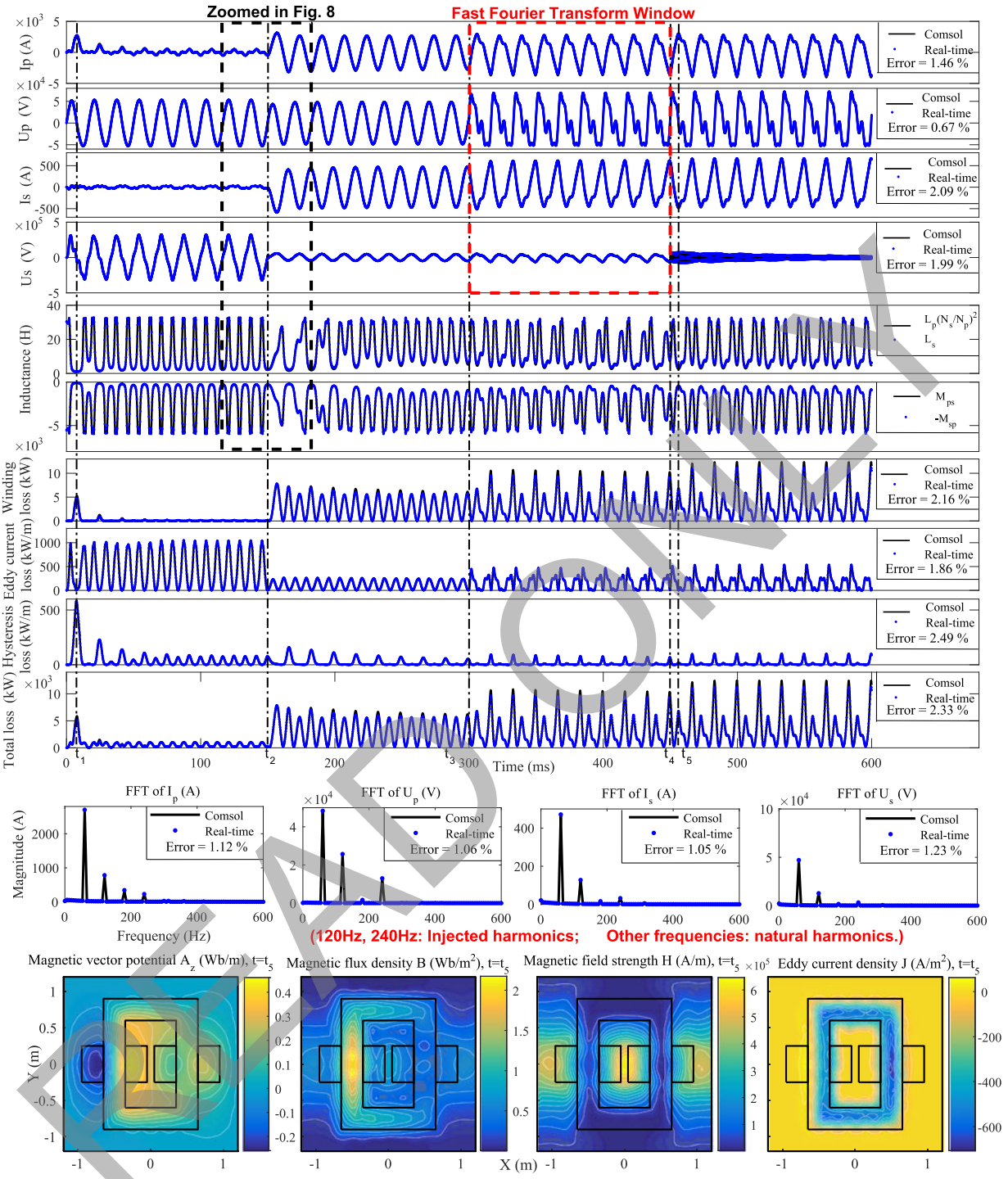

Fig. 12. Real-time simulation results and the comparison with Comsol off-line results for **multi-rate** Case Study II: time-domain, frequency-domain, and field distributions.

real-time FE model can be easily coupled to a larger complicated external network, which can be solved independently with the accurate inductances obtained from the FE model. When applied for complex geometries that require increasing the number of nodes and elements, the resource usage of the *Assemble Current* and the *Newton Solver* hardware blocks remains unchanged and only the pipelined loop count increases, and the hardware resources usage and latency of other blocks increase linearly or logarithmically.

V. Conclusion

In this paper, real-time finite-element computation of electromagnetic transients in a transformer is attempted for the first time. The transmission line modeling method successfully

decoupled the nonlinear elements from the linear network so that the computation can be massively parallelized. The parallelism of the different phases of the TLM technique is fully explored and implemented on a FPGA board with deep data pipelining. The proposed field-circuit coupling enabled the real-time FE model to effectively interface with external network to capture the transient behavior of interest. Tests conducted in comparison with a commercial FEM package prove excellent accuracy and computational efficiency of the real-time FEM approach, which provides unprecedented data detail of the simulated transformer.

Potential applications of the proposed real-time FE model are many, allowing detailed modeling of the power transformer in AC and DC networks. Although the presented work focused on the 2D modeling of a single-phase transformer, the proposed approach can be extended to 2D or 3D modeling of multi-phase multi-winding transformers.

APPENDIX

Preisach model: $a_0 = a_1 = 0$, $b_0 = b_1 = 3162$, $c = 0.6$.

Transformer parameters: The transformer size is 1.3 m $\times$ 1.8 m for the outer rectangle and 0.7 m $\times$ 1.2 m for the inner. The coil size is 0.3 m $\times$ 0.5 m, and the number of coil turns is 200 for the primary side and 1076 for the secondary. $\mathrm{R_p} = 0.667\ \Omega, \mathrm{R_s} = 3.588\ \Omega$ and $\sigma^e = 1000$.

Case study parameters: $\mathrm{V_{ac}} = 37.5\sqrt{2}\sin(120\pi\mathrm{t})\mathrm{kV}$, $\mathrm{R_1} = 5\Omega, \mathrm{L_1} = 2$ mH, $\mathrm{R_{L1}} = 200\ \Omega, \mathrm{R_{L2}} = 100\ \Omega, \mathrm{L_{L1}} = 10$ mH and $\mathrm{L_{L2}} = 5$ mH. The length of the transmission line TL is 15 km, travelling time is 50 μs and characteristic impedance Z_{TL} is 200 Ω. The magnitude of the injected second and fourth harmonics are 9.38 kV and 4.69 kV respectively.

REFERENCES

[1] J. A. Martinez and B. A. Mork, "Transformer modeling for low- and mid-frequency transients—A review," *IEEE Trans. Power Del.*, vol. 22, no. 2, pp. 1235–1246, Apr. 2007.

[2] V. Brandwajn, H. W. Dommel, and I. I. Dommel, "Matrix representation of three-phase n-winding transformers for steady-state and transient studies," *IEEE Trans. Power App. Syst.*, vol. PAS-101, no. 6, pp. 1369–1378, Jun. 1982.

[3] F. de Leon and A. Semlyen, "Complete transformer model for electromagnetic transients," *IEEE Trans. Power Del.*, vol. 9, no. 1, pp. 231–239, Jan. 1994.

[4] N. D. Hatziargyriou, J. M. Prousalidis, and B. C. Papadias, "Generalised transformer model based on the analysis of its magnetic core circuit," *IET Gen., Transm. Distrib*, vol. 140, no. 4, pp. 269–278, Jul. 1993.

[5] A. Narang and R. H. Brierley, "Topology based magnetic model for steady-state and transient studies for three-phase core type transformers," *IEEE Trans. Power Syst.*, vol. 9, no. 3, pp. 1337–1349, Aug. 1994.

[6] J. Arrillaga, W. Enright, N. R. Watson, and A. R. Wood, "Improved simulation of HVDC converter transformers in electromagnetic transient programs," *IET Gen., Transm. Distrib.*, vol. 144, no. 2, pp. 100–106, Mar. 1997.

[7] J. Liu and V. Dinavahi, "A real-time nonlinear hysteretic power transformer transient model on FPGA," *IEEE Trans. Ind. Electron.*, vol. 61, no. 7, pp. 3587–3597, Jul. 2014.

[8] J. Liu and V. Dinavahi, "Nonlinear magnetic equivalent circuit-based real-time sen transformer electromagnetic transient model on FPGA for HIL emulation," *IEEE Trans. Power Del.*, vol. 31, no. 6, pp. 2483–2493, Dec. 2016.

[9] P. B. Johns and R. L. Beurle, "Numerical solution of 2-dimensional scattering problems using a transmission-line matrix," *Proc. Inst. Elect. Eng.*, vol. 118, no. 9, pp. 1203–1208, Sep. 1971.

[10] P. B. Johns and M. O'Brien, "Use of the transmission-line modelling (t.l.m.) method to solve non-linear lumped networks," *Radio Electron. Eng.*, vol. 50, no. 1.2, pp. 59–70, Jan. 1980.

[11] W. J. R. Hoefer, "The transmission-line matrix method - theory and applications," *IEEE Trans. Microw. Theory Techn.*, vol. MTT-33, no. 10, pp. 882–893, Oct. 1985.

[12] S. Y. R. Hui and C. Christopoulos, "Numerical simulation of power circuits using transmission-line modelling" *Proc. Inst. Elect. Eng., Phys. Sci., Meas. Instrum., Manage. Educ.*, vol. 137, no. 6, Nov. 1990, pp. 379–384.

[13] V. Dinavahi, "Transient analysis of systems with multiple nonlinear elements using TLM," *IEEE Trans. Power Syst.*, vol. 19, no. 4, pp. 2102–2103, Nov. 2004.

[14] B. Asghari and V. Dinavahi, "Real-time nonlinear transient simulation based on optimized transmission line modeling," *IEEE Trans. Power Syst.*, vol. 26, no. 2, pp. 699–709, May 2011.

[15] J. Lobry, J. Trecat, and C. Broche, "The transmission line modeling (TLM) method as a new iterative technique in nonlinear 2-d magnetostatics," *IEEE Trans. Magn.*, vol. 32, no. 2, pp. 559–566, Mar. 1996.

[16] O. Deblecker, J. Lobry, and C. Broche, "Use of transmission-line modelling method in FEM for solution of nonlinear eddy-current problems," *Proc. Inst. Elect. Sci., Meas. Technol.*, vol. 145, no. 1, Jan. 1998, pp. 31–38.

[17] O. Deblecker, J. Lobry, and C. Broche, "Novel algorithm based on transmission-line modeling in the finite-element method for nonlinear quasi-static field analysis," *IEEE Trans. Magn.*, vol. 39, no. 1, pp. 529–538, Jan. 2003.

[18] O. C. Zienkiewicz, R. L. Taylor, and J. Z. Zhu, *The Finite Element Method*, 6th ed. Amsterdam, The Netherlands: Elsevier, 2005.

[19] I. D. Mayergoyz, *Mathematical Models of Hysteresis*. Berlin, Germany: Springer-Verlag, 1991.

[20] J. Fuzi, "Analytical approximation of Preisach distribution functions," *IEEE Trans. Magn.*, vol. 39, no. 3, pp. 1357–1360, May 2003.

[21] B. Asghari, V. Dinavahi, M. Rioual, J. A. Martinez, and R. Iravani, "Interfacing techniques for electromagnetic field and circuit simulation programs ieee task force on interfacing techniques for simulation tools," *IEEE Trans. Power Del.*, vol. 24, no. 2, pp. 939–950, Apr. 2009.

[22] P. Lombard and G. Meunier, "A general method for electric and magnetic coupled problem in 2d and magnetodynamic domain," *IEEE Trans. Magn.*, vol. 28, no. 2, pp. 1291–1294, Mar. 1992.

[23] H. W. Dommel, "Digital computer solution of electromagnetic transients in single-and multiphase networks," *IEEE Trans. Power App. Syst.*, vol. PAS-88, no. 4, pp. 388–399, Apr. 1969.

Peng Liu (S'15) received the B.Sc. and M.Eng. degrees in electrical engineering from Harbin Institute of Technology, Harbin, China, in 2013 and 2015, respectively. He is currently working toward the Ph.D. degree at the Department of Electrical and Computer Engineering, University of Alberta, Edmonton, AB, Canada. His research interests include computational electromagnetics, real-time simulation, and parallel and distributed processing.

Venkata Dinavahi (S'94–M'00–SM'08) received the B.Eng. degree in electrical engineering from Visvesvaraya National Institute of Technology, Nagpur, Nagpur, India, in 1993, the M.Tech degree in electrical engineering from the Indian Institute of Technology Kanpur, Kanpur, India, in 1996, and the Ph.D. degree in electrical and computer engineering from the University of Toronto, Toronto, ON, Canada, in 2000. He is currently a Professor with the Department of Electrical and Computer Engineering, University of Alberta, Edmonton, AB, Canada. His research interests include real-time simulation of power systems and power electronic systems, electromagnetic transients, device-level modeling, large-scale systems, and parallel and distributed computing.